TOPICAL REVIEW — Topological electronic states

Quantum anomalous Hall effect in real materials*

Jiayong Zhang(张加永)[1], Bao Zhao(赵宝)[1], Tong Zhou(周通)[1], and Zhongqin Yang(杨中芹)[1,2,†]

[1] State Key Laboratory of Surface Physics and Key Laboratory for Computational Physical Sciences (MOE) & Department of Physics, Fudan University, Shanghai 200433, China

[2] Collaborative Innovation Center of Advanced Microstructures, Fudan University, Shanghai 200433, China

(Received 25 February 2016; revised manuscript received 8 May 2016; published online 28 September 2016)

Under a strong magnetic field, the quantum Hall (QH) effect can be observed in two-dimensional electronic gas systems. If the quantized Hall conductivity is acquired in a system without the need of an external magnetic field, then it will give rise to a new quantum state, the quantum anomalous Hall (QAH) state. The QAH state is a novel quantum state that is insulating in the bulk but exhibits unique conducting edge states topologically protected from backscattering and holds great potential for applications in low-power-consumption electronics. The realization of the QAH effect in real materials is of great significance. In this paper, we systematically review the theoretical proposals that have been brought forward to realize the QAH effect in various real material systems or structures, including magnetically doped topological insulators, graphene-based systems, silicene-based systems, two-dimensional organometallic frameworks, quantum wells, and functionalized Sb(111) monolayers, etc. Our paper can help our readers to quickly grasp the recent developments in this field.

Keywords: quantum anomalous Hall effect, topological insulator, ferromagnetic insulator, two-dimensional material

PACS: 73.43.–f, 71.70.Ej, 73.22.–f, 72.25.Dc **DOI:** 10.1088/1674-1056/25/11/117308

1. Introduction

Topological states are insulating in the bulk but exhibit robust conducting boundary states topologically protected from backscattering. Recently, finding these topologically nontrivial states in realistic material systems has become one of the fastest developing research directions in condensed matter physics and materials science.[1–6] In a two-dimensional (2D) electron gas, quantum Hall (QH) effect,[7] which was later called the first category of the topological states, can be observed by applying an external strong magnetic field to the system, breaking the time reversal symmetry (TRS) of the system. Actually, internal magnetization can also break the TRS of a system without the need of an external magnetic field. When coupled with special band structures and spin–orbit coupling (SOC) of the system, it can generate the so called quantum anomalous Hall (QAH) effect, which was first proposed by Haldane.[8] The realization of QAH effects in realistic material systems may greatly promote the development of low-power-consumption electronics. So far, a number of theoretical proposals have been raised to produce the QAH effect,[9–34] such as mercury-based quantum walls,[9] thin films of magnetically doped topological insulators (TIs),[11] graphene and silicene based systems,[12–21] organic TIs,[22] (111) bilayers of $LaCoO_3$,[25] and so on. The topology of a QAH state is characterized by the appearance of a quantized Hall conductivity in the absence of an external magnetic field.

To acquire QAH insulators, the following four conditions should be satisfied simultaneously: 2D systems, insulators, long-range ferromagnetic (FM) order, and special band structures with finite Chern number. In general, one real material may solely satisfy one or two of the above conditions. In particular, the insulators in nature usually have the antiferromagnetic (AFM) order instead of the FM order. Thus, real materials need to be designed and reconstructed to present the QAH effect. The finite Chern number is usually triggered by SOC interactions in the system. Forming an FM order in a 2D insulating film through magnetic doping is a classical route to produce the QAH effect. For example, the experimental realization of the QAH effect was reported in thin films of Cr- or V-doped $(Bi,Sb)_2Te_3$ topological insulators.[35–38] Actually, both the experimental and theoretical researches indicate that introducing a long-range FM order in insulating films is one of the toughest tasks in carrying out experiments with the QAH effect. Some theoretical studies have shown that the TRS of the 2D systems can be broken by introducing a magnetic exchange field through doping (adsorbing) transition-metal (TM) atoms[11,12] or proximity coupling to an FM or AFM insulator.[16–18]

In this paper, we systematically review the theoretical proposals that have been brought forward to produce the QAH effect in realistic material systems. In Section 2, we review

*Project supported by the National Basic Research Program of China (Grant No. 2011CB921803), the National Natural Science Foundation of China (Grant No. 11574051), the Natural Science Foundation of Shanghai, China (Grant No. 14ZR1403400), and Fudan High-end Computing Center, China.

†Corresponding author. E-mail: zyang@fudan.edu.cn

© 2016 Chinese Physical Society and IOP Publishing Ltd

the work of realizing the QAH effect by doping TM atoms in topological insulators. In Section 3, we introduce the theoretical model of realizing the QAH effect in graphene, and review the work of achieving the QAH effect in graphene-based systems. Silicene is a monolayer of silicon atoms with a buckled honeycomb structure but which still possesses the Dirac electronic properties, like graphene. How to realize the QAH effect in silicene-based systems is given in Section 4. In Section 5, we review the QAH effect studied in several other systems, including 2D organic topological insulators and square or triangular lattice systems, etc. In Section 6, we briefly introduce some new topological states proposed based on the QAH effect, including valley-polarized quantum anomalous Hall (VP-QAH) state and quantum spin-quantum anomalous Hall (QSQAH) state. Our conclusions and outlook are given in Section 7.

2. QAH effect in magnetic atom doped topological insulator films

The QAH effect may be realized in a topological insulator film with quantum spin Hall (QSH) effect by breaking its TRS. If one spin state in the system is in the inverted regime and the other spin state is in the normal regime, then the inverted spin state may give a topologically nontrivial insulating state with a quantized Hall conductivity and the system will become a QAH effect insulator, indicating the QAH state closely related to the QSH state. The theoretical models and first-principles calculations showed that the QAH state can indeed be realized in the TRS-breaking topological insulator films by doping magnetic atoms.[9–11] Some typical examples are illustrated in the following.

The HgTe quantum well (QW) is a well-known QSH effect insulator,[39] which has been observed in experiments.[40] Liu *et al.* proposed that the QAH effect can be observed in the TRS-breaking HgTe QWs.[9] To obtain the QAH effect, the system must satisfy two conditions: (i) the state with one kind of spin is in the inverted regime while the other is in the normal regime, (ii) the entire system is still in the insulating state with a bulk band gap. The above conditions are illustrated in Fig. 1(a), and the physics can be understood from the edge states picture (Fig. 1(b)). The counter propagating edge states carrying opposite spins will appear on the boundary of the QSH insulator. With the increase of the spin splitting term, one of the two spin states (the spin-down edge state) will experience a topological phase transition. The spin-down edge states penetrate much deeper into the bulk due to the decreasing gap and eventually disappear, leaving only the spin-up edge states bound more strongly to the edge. Thus, the system has only the spin-up edge states and transforms from the QSH state to the QAH state.[9] Therefore, a QAH effect insulator can be achieved from a QSH effect insulator by introducing a TRS-breaking perturbation. For the HgTe QWs, the theoretical study predicted that the TRS could be broken by doping Mn atoms, and the QAH effect existed in this system as long as the Mn spins were polarized.[9] Besides, based on first-principles calculations, Zhang *et al.* predicted that the junction wells comprising II–VI, III–V, or IV semiconductors were a large class of new QSH effect insulators, and the transition from the QSH state to the QAH state could also be realized by breaking the TRS through doping magnetic atoms.[10]

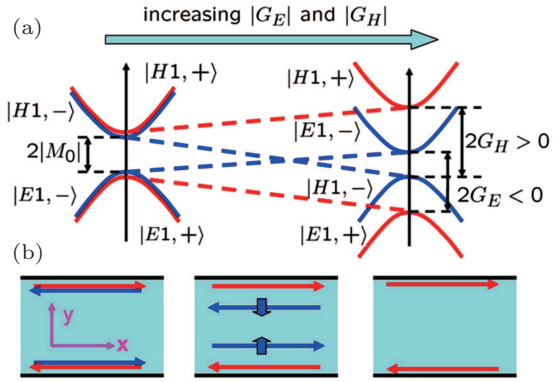


Fig. 1. (color online) Evolution of band structure and edge states upon increasing the spin splitting. (a) The spin-down states $|E1,-\rangle$ and $|H1,-\rangle$ in the same block of the Hamiltonian (Eq. (1) from Ref. [6]) touch each other and then enter the normal regime. In panel (b), the behavior of the edge states during the level crossing in the case of panel (a) is shown. Reprinted with permission from Ref. [9]. Copyright 2008 by the American Physical Society.

The tetradymite semiconductors Bi_2Te_3, Bi_2Se_3, and Sb_2Te_3 are also a well-known class of topological insulators.[41] Yu *et al.* predicted that thin films made out of this family of compounds doped with proper magnetic atoms (Cr or Fe) supported the QAH state.[11] The physical mechanism of realizing the QAH effect in the thin-film topological insulator systems with FM ordering is illustrated in Fig. 2. The TRS can be broken by introducing a magnetic exchange field, and the Chern number of one of the two spin states can be changed by a large exchange field. As displayed in Fig. 2(a), the four-band system is originally in the topologically trivial phase. When a large exchange field is included, the band inversion will be induced in the upper block and the two subbands in the lower block will be pushed even farther away from each other. After the SOC is considered, a bulk band gap will be opened and the 2D model with a negative mass in the upper block gives the integer Hall conductivity of e^2/h, indicating the realization of the QAH effect. Figure 2(b) shows the case when the system is originally in the topological nontrivial phase, where the inverted band structures exist in both of the two blocks. In this case, the band inversion in the upper block can be increased and in the lower block can be released by a sufficiently large exchange field. The bulk band gap will also be induced after including the SOC and the negative

mass in the upper block gives a quantized Hall conductivity of e^2/h.[11] The QAH effect in this proposal is robust, compared to the above HgMnTe QWs system in which a further assumption that the hole and electron sub-bands have opposite signs of the exchange splitting is required.[9,11] Based on this theoretical proposal (Fig. 2), the first experimental observation of the QAH effect was realized in a magnetic topological insulator of Cr-doped $(Bi,Sb)_2Te_3$ thin films[35] in 2013. However, the experimental realization of the QAH effect in thin films of magnetically doped topological insulators[35–38] is still full of challenges and the observation temperature is very low (such as 30 milli-Kelvin[35]), which is probably associated with the unavoidable disorder effect due to the extreme concentration of magnetic dopants.

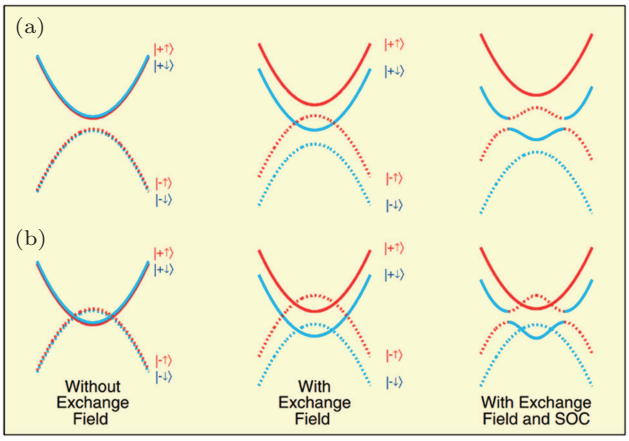


Fig. 2. (color online) Evolution of the sub-band structure upon increasing the exchange field. The solid lines denote the sub-bands that have even parity at Γ point, and the dashed lines denote the sub-bands with odd parity at Γ point. The blue (red) color denotes the spin-down (spin-up) electrons. (a) The initial sub-bands are not inverted. When the exchange field is strong enough, a pair of inverted sub-bands appear (red dashed line and blue solid line). (b) The initial sub-bands are already inverted. The exchange field releases the band inversion in one pair of sub-bands (red solid line and blue dashed line) and increases the band inversion in the other pair (red dashed line and blue solid line). Reprinted with permission from Ref. [11]. Copyright 2010 by the American Association for the Advancement Science.

3. QAH effect in graphene-based systems

Graphene, which is a fascinating 2D material with a honeycomb lattice, special Dirac-cone electronic properties, and relatively mature technologies of sample growth and device fabrication, has become a prototype material for engineering the QAH effect.[12–18] Theoretical studies show that a nontrivial QAH band gap in graphene-based systems can be opened near the Dirac points in the presence of both Rashba spin–orbit coupling and magnetic exchange field.[12,13] We now introduce the physical mechanism of the gap opening and the QAH effect in graphene through the tight-binding (TB) model.[12] The TB Hamiltonian for graphene with the consideration of Rashba SOC and magnetic exchange field can be written as[12]

$$H = -t\sum_{\langle ij\rangle\alpha} c^{\dagger}_{i\alpha}c_{j\alpha} + \mathrm{i}t_{\mathrm{SO}}\sum_{\langle ij\rangle\alpha\beta}\hat{\boldsymbol{e}}_z\cdot\left(\boldsymbol{\sigma}_{\alpha\beta}\times\boldsymbol{d}_{ij}\right)^{z}_{\alpha\beta}c^{\dagger}_{i\alpha}c_{j\beta} + \lambda\sum_{i\alpha}c^{\dagger}_{i\alpha}\sigma_z c_{i\alpha}, \quad (1)$$

where $c^{\dagger}_{i\alpha}$ ($c_{i\alpha}$) creates (annihilates) an electron with spin α on site i, $\langle i,j\rangle$ runs over all the nearest-neighboring hopping sites, $\boldsymbol{\sigma}$ is the Pauli matrix, and $\boldsymbol{d}_{ij}$ denotes the lattice vector pointing from site j to site i. In Eq. (1), the first term describes the nearest-neighbor hopping, and the second and the third terms represent the Rashba SOC and the magnetic exchange field, respectively.

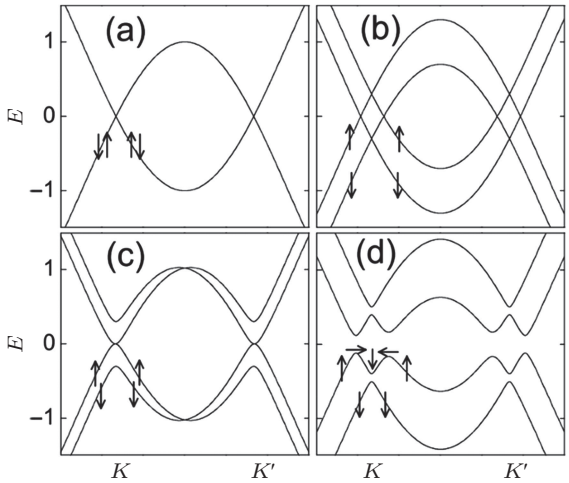


Fig. 3. Evolution of band structures of bulk graphene along the profile of $k_y = 0$. The arrows represent the spin directions. (a) Pristine graphene: spin-up and spin-down states are degenerate; (b) when only exchange field $\lambda = 0.4$ is applied, the spin-up/spin-down bands are upward/downward lifted with the four bands crossing near K and K' points; (c) when only Rashba SOC $t_{\mathrm{SO}} = 0.1$ is present, the spin-up and spin-down states are mixed around the band crossing points; (d) when both exchange field $\lambda = 0.4$ and Rashba SOC $t_{\mathrm{SO}} = 0.1$ are present, a bulk gap is opened and all four bands become nondegenerate. Reprinted with permission from Ref. [12]. Copyright 2010 by the American Physical Society.

Figure 3 shows the evolution of the band structures of graphene obtained from the above TB Hamiltonian with Rashba SOC t_{SO} and exchange field λ.[12] Figure 3(a) plots the band structure of pristine graphene with the perfect Dirac bands located at the K and K' points. The K and K' points are four-fold degenerate, while the other points are doubly degenerate due to the spin degeneracy. When only the exchange field is included, the spin-up and spin-down Dirac bands around the K and K' points will cross with each other (Fig. 3(b)). Thus, a bulk band gap can be opened at the band-crossing points when both Rashba SOC and exchange field are considered (Fig. 3(d)). This SOC-induced insulting state is topologically nontrivial and exhibits the quantized charge Hall conductivity, which can be identified by calculating the Berry curvature and the Chern number. The Berry curvature $\Omega(\boldsymbol{k})$ is calculated as:[42–44]

$$\Omega(\boldsymbol{k}) = \sum_n f_n\Omega_n(\boldsymbol{k}),$$

$$\Omega_n(\boldsymbol{k}) = -2\mathrm{Im}\sum_{m\neq n}\frac{\hbar^2\langle\psi_{n\boldsymbol{k}}|v_x|\psi_{m\boldsymbol{k}}\rangle\langle\psi_{m\boldsymbol{k}}|v_y|\psi_{n\boldsymbol{k}}\rangle}{(E_m - E_n)^2}, \quad (2)$$

where E_n is the eigenvalue of the Bloch functions $|\psi_{n\boldsymbol{k}}\rangle$, $v_{x(y)}$ are the velocity operators, f_n is the Fermi–Dirac distribution function, and the summation is over all of the occupied states. By integrating the Berry curvature over the first Brillouin zone (BZ), the Chern number C and Hall conductivity σ_{xy} can be obtained as $C = \frac{1}{2\pi}\sum_n \int_{\mathrm{BZ}} \mathrm{d}^2k\Omega_n$ and $\sigma_{xy} = Ce^2/h$. The absolute value of the Chern number corresponds to the number of gapless chiral edge states along each side of the sample.

The above band evolution clearly shows the physical mechanism of realizing the QAH effect in the graphene system, indicating that graphene is an ideal system for applications of the QAH effect. In consideration of the fact that graphene has extremely weak intrinsic SOC,[45,46] both the magnetic exchange field and the SOC should be induced externally to realize the QAH effect in graphene. We now introduce the theoretical proposals of achieving the QAH effect in the graphene-based systems through adsorbing TM atoms[12,14] and proximity coupling to magnetic insulators.[16–18]

3.1. QAH effect in graphene via transition-metal-atom adsorption

To realize the QAH effect in the graphene system, the time-reversal symmetry must be broken and the Rashba SOC must be enlarged.[12] The time-reversal symmetry of graphene can be broken by introducing an external magnetic exchange field through adsorbing TM atoms.[12–14] Besides, when adsorbing low-concentration TM atoms on the graphene sheet, the interaction between the magnetic adatoms and the π orbital of graphene, occurring on one side of graphene, will induce a sizeable Rashba SOC.[47] The first-principles calculations show that the QAH effect can be realized in graphene via adsorbing appropriate TM atoms at the hollow adsorption sites of the graphene supercell.[14] We take the case of Fe adsorbed at the hollow adsorption site of the 4×4 supercell of graphene as an example to illustrate the above proposal.[12] Figure 4(a) shows the atomic structure of one Fe atom adsorbed at the hollow site of the 4×4 supercell of graphene. The calculated band structures show that the magnetic exchange field is induced in graphene by the Fe atoms and a bulk band gap is indeed opened at the crossing points of the spin-up and spin-down bands. Figures 4(e) and 4(f) plot the calculated Berry curvature $\Omega(\boldsymbol{k})$ along the high-symmetry lines. Most of the nonzero $\Omega(\boldsymbol{k})$ only locates at the SOC-induced band gaps around the K and K' points with the same sign. By integrating $\Omega(\boldsymbol{k})$ over the first BZ, the nonzero integer Chern number $C = 2$ is obtained, indicating that the QAH effect is realized in this system. The opened nontrivial bulk band gap is not small (about 5.5 meV) due to the enlarged Rashba SOC by the adsorption of Fe atoms, which is accessible under current experimental conditions.[12]

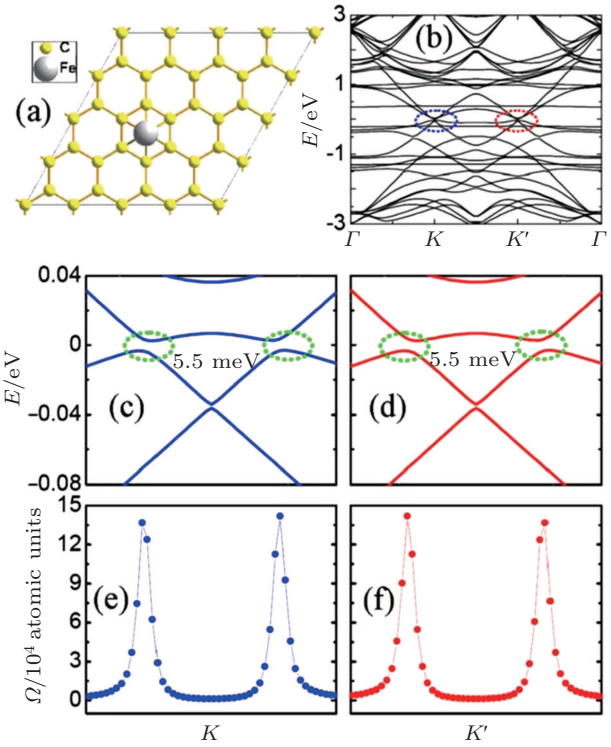


Fig. 4. (color online) (a) Typical structure geometry of a Fe atom on top of the hollow position of a 4×4 supercell of graphene. (b) Bulk band structure with SOC included along the high symmetry lines. The Fermi level is exactly located in the gap. (c) and (d) Zoom-in plots of the band structure at K and K' points, respectively. Gaps of ~ 5.5 meV, circled by the green dotted curves, are opened. (e) and (f) Berry curvature distribution Ω of the valence bands near K and K' points. The Berry curvatures at K and K' share the same sign, thus giving a nonzero Chern number. Reprinted with permission from Ref. [12]. Copyright 2010 by the American Physical Society.

3.2. QAH effect in graphene proximity coupled to antiferromagnetic insulators

The above theoretical proposal shows that the QAH effect can be realized in graphene by depositing low-concentration TM atoms. The adsorption energies of the TM atoms on

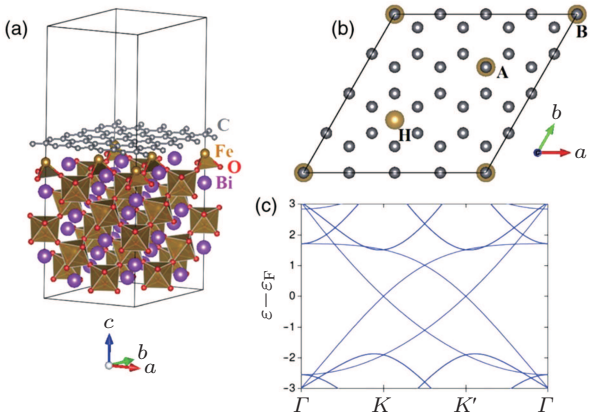


Fig. 5. (color online) (a) Supercell for graphene on a (111) $BiFeO_3$ surface. Gray (the top layer), purple (large), yellow (medium), and red (small) colors represent C, Bi, Fe, and O atoms, respectively. (b) A top view of graphene with one layer of iron atoms. One Fe atom is located at the hollow site labeled by H, while the other two Fe atoms are located at the top sites labeled by A and B. (c) Band structure along high symmetry lines for a 4×4 supercell of graphene. Reprinted with permission from Ref. [16]. Copyright 2014 by the American Physical Society.

graphene are, however, usually very small.[14] Thus, the TM atoms tend to gather into clusters[48,49] and the long-range FM order may not survive as expected, which make it particular difficult to realize the QAH effect in TM atoms decorated graphene systems in experiments. Besides depositing TM atoms, the ferromagnetism can also be induced by proximity coupling graphene to an FM insulator, which may overcome the above mentioned problems. Depositing graphene on a magnetic substrate can induce both the magnetic exchange field and considerable Rashba SOC, essential for the realization of the QAH effect. $BiFeO_3$ has a perovskite structure and is a G-type antiferromagnet. When graphene is deposited on the (111) surface of $BiFeO_3$ with Fe terminal (Fig. 5), the nearest-neighboring FM Fe plane will induce a strong homogeneous magnetic exchange field in the graphene layer. Qiao *et al.* proposed that the QAH effect can be realized in graphene proximity coupled to the (111) surface of the G-type AFM insulator $BiFeO_3$ with the combination configuration shown in Fig. 5(b). The long-range FM order and the relatively large Rashba SOC are both well preserved in the top layer graphene.[16] The band structures in Fig. 6 show that the Dirac points of graphene just locate inside the bulk band gap of the substrate and a bulk band gap of about 1.1 meV is opened at the crossing points of the spin-up and spin-down Dirac bands after considering the SOC.

$RbMnCl_3$ is an AFM insulator with the Mn sites forming alternating (001) FM planes, and it also has a hexagonal structure[50] as the graphene does, which makes the experimental fabrication of the heterostructure of graphene on the (001) surface of $RbMnCl_3$ easy. Based on first-principles calculations, Zhang *et al.* showed that the QAH effect could be realized in the heterostructure of graphene on the AFM insulator $RbMnCl_3$ with Mn terminal.[17]

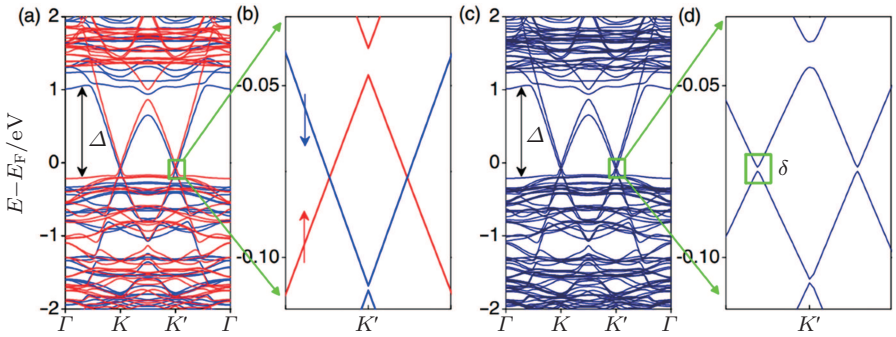


Fig. 6. (color online) Bulk band structures of graphene on $BiFeO_3$. (a) Spin-resolved band structures. (b) Zoom in on the green box of panel (a). The blue (thin) and red (thick) lines in panels (a) and (b) represent the spin-up and spin-down bands, respectively. (c) Band structure when the spin–orbit coupling is included. A bulk gap δ of about 1.1 meV is centered on the avoided crossings near the K and K' valleys. Note that the nontrivial band gap δ is inside the bulk gap Δ of $BiFeO_3$. (d) Zoom in on the green box of panel (c). Reprinted with permission from Ref. [16]. Copyright 2014 by the American Physical Society.

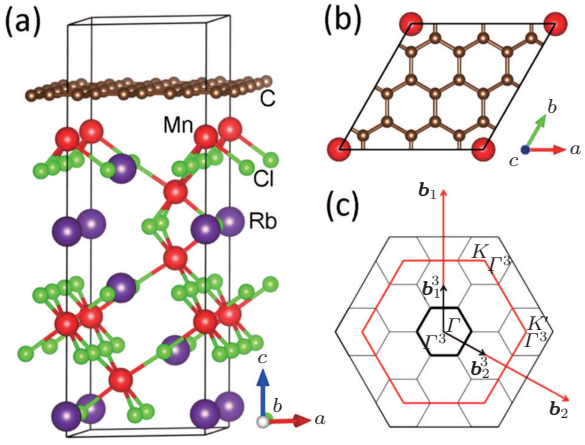


Fig. 7. (color online) (a) Side view of the heterostructure with graphene on a (001) $RbMnCl_3$ surface. The C, Rb, Mn, and Cl atoms are denoted in brown, purple, red, and green, respectively. (b) Top view of the heterostructure with the topmost layer Mn atoms of the $MnRbCl_3$ located at the hollow site of graphene. For clarity, only graphene and the topmost layer Mn atoms are displayed. (c) The reciprocal momentum space structures for the 1×1 and 3×3 supercells of graphene, where $\boldsymbol{b}_{1,2}$ and $\boldsymbol{b}^3_{1,2}$ are the reciprocal vectors of the 1×1 and 3×3 supercells, respectively. K and K' points of the 3×3 supercell of graphene are folded into the Γ point. Reprinted with permission from Ref. [17]. Copyright 2015 by Nature Publication Group.

In their first-principles calculations, a 3×3 supercell of graphene was employed to match the (001) surface of $RbMnCl_3$ with Mn terminal, as shown in Fig. 7(a).[17] In contrast from the cases of the 1×1 and 4×4 supercells, the K and K' points for the 3×3 supercell of graphene are both folded into the Γ point (as illustrated in Fig. 7(c)). When the graphene is deposited on the (001) surface of the $RbMnCl_3$ substrate, through the proximity effect, the topmost FM Mn layer in $RbMnCl_3$ will induce a strong magnetic exchange field in graphene, which makes the spin-up and spin-down bands of the π states of graphene cross with each other around the Dirac point. Besides, the Dirac bands are just located inside the bulk band gap of the substrate. The crossing of spin-up and spin-down Dirac bands induced by the magnetic exchange field is essential to the QAH effect.[12] A bulk band gap of about 1.2 meV is opened at the bands crossing points after the SOC is included (Fig. 8(a)). The size of the gap is much larger than the topologically nontrivial gap of pure graphene[45,46] due to the enhanced Rashba SOC through the interaction be-

tween graphene and the $RbMnCl_3$ substrate. The peaks of the calculated Berry curvature $\Omega(\boldsymbol{k})$ only locate around the SOC-induced band gaps (Figs. 8(a) and 8(b)). The Chern number $C = 2$ is obtained for the system, meaning two chiral edge channels will arise on each side of the sample and confirming the realization of the QAH effect in the graphene/$RbMnCl_3$ heterostructure.[17] As shown in Fig. 8(d), the QAH gap can be greatly increased by enhancing the interaction between graphene and the substrate.

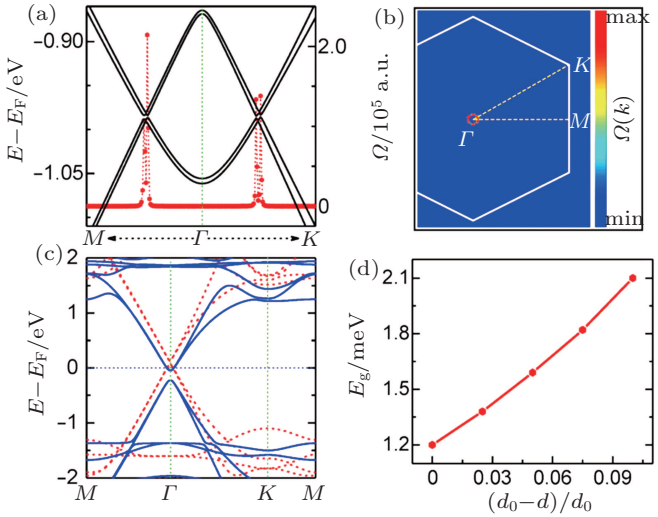


Fig. 8. (color online) (a) The band structure (black solid curves) and the Berry curvature (red dotted curve) of the graphene/$RbMnCl_3$ heterostructure. (b) The 2D distribution of the Berry curvature in the momentum space, located primarily around the Γ point. (c) The bulk band structure of the graphene/$RbMnCl_3$ heterostructure with an extra hole in the supercell. (d) The bulk band gap E_g as a function of $(d_0 - d)/d_0$, where d is the distance between graphene and the $RbMnCl_3$ film and d_0 is the corresponding optimized distance. Reprinted with permission from Ref. [17]. Copyright 2015 by Nature Publication Group.

3.3. Robust QAH effect in graphene-based van der Waals heterostructures

As discussed above, the QAH effect can emerge in graphene by depositing it onto a suitable magnetic substrate. The hidden challenge in such proposals is, however, that the QAH effect depends quite sensitively on the combination configuration of graphene and the substrate. The QAH effect may be quenched if the pattern between graphene and the substrate is varied slightly, making the experimental observation very difficult. A recent first-principles study of graphene on a layered FM insulator $Cr_2Ge_2Te_6$ has solved this problem.[18] The system of graphene on a $Cr_2Ge_2Te_6$ film belongs to a special structure, called van der Waals (vdW) heterostructures,[51,52] due to the vdW interaction between the graphene and the substrate. This category of heterostructures is found to own several fantastic characteristics beneficial to realizing the QAH effect in experiments.

$Cr_2Ge_2Te_6$ is an FM insulator with a relatively high Curie temperature of 61 K.[53] The hexagonal structure of $Cr_2Ge_2Te_6$ matches very well with that of graphene. Particularly, the $Cr_2Ge_2Te_6$ bulk is layered with the adjacent planes joined by vdW bonds. The $Cr_2Ge_2Te_6$ films of very high quality have been successfully fabricated in experiments.[54,55] When the graphene is deposited on the 2D exfoliated film of $Cr_2Ge_2Te_6$, a vdW heterostructure is formed.[51] The exotic feature of this system is that the achieved QAH effect is independent of the stacking patterns between graphene and the FM substrate. This robustness makes the experimental observation highly accessible. The Fermi level (E_F) is found to be located exactly inside the nontrivial bulk band gap, favorable to the transport measurement of the QAH effect. The nontrivial bulk band gap can be tuned flexibly by varying the vdW gap between graphene and the substrate.

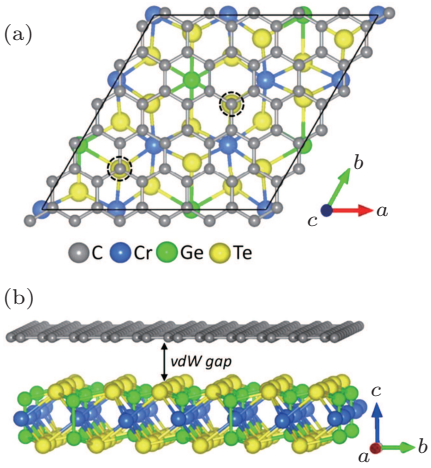


Fig. 9. (color online) Top (a) and side (b) views of one of the vdW heterostructures of graphene on a monolayer $Cr_2Ge_2Te_6$. In the unit cell, two C atoms of graphene lie directly above two Te atoms (labeled by dashed circles) of $Cr_2Ge_2Te_6$. Reprinted with permission from Ref. [18]. Copyright 2015 by the American Physical Society.

Figure 9 shows the atomistic structure of the heterostructure, where graphene is deposited on a monolayer $Cr_2Ge_2Te_6$. According to the first-principles calculations,[18] the optimized distance between graphene and the monolayer $Cr_2Ge_2Te_6$ is 3.56 Å, which together with the small cohesive energy implies that this kind of heterostructure is a vdW heterostructure, relatively straightforward to fabricate in experiments.[51] The magnetic exchange field can indeed be induced in the graphene sheet through the proximity effect by the FM insulator substrate $Cr_2Ge_2Te_6$, as shown in the spin-polarized band structures (Figs. 10(a) and 10(b)). The Dirac bands of the graphene are located just inside the bulk band gap of the $Cr_2Ge_2Te_6$ substrate. When the SOC is included, an energy gap is opened at the crossing points of the crossing bands with opposite spin orientations, just around E_F (Figs. 10(c) and 10(d)). The gap is about 0.5 meV, much larger than the topologically nontrivial band gap of pure graphene. The calculated Berry curvatures and Chern number $(C = 2)$ confirm that the SOC-induced insulating state in the vdW heterostructure is the QAH state. The calculated edge states at an armchair edge of the semi-infinite heterostructure system (Fig. 11(b)) shows that two chiral charge conducting channels will appear on each side of the sample, consistent with the obtained Chern number $C = 2$.[18]

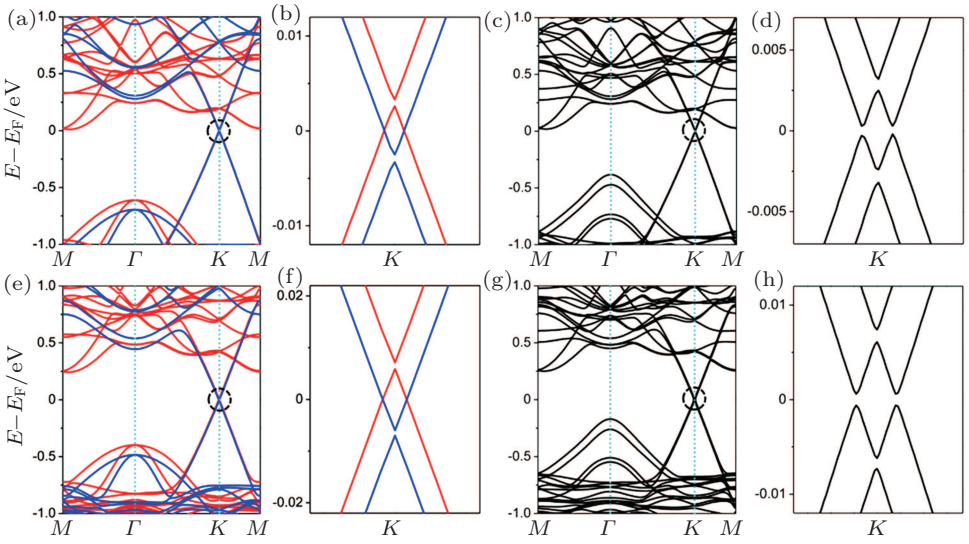


Fig. 10. (color online) (a), (c) The calculated band structures of the vdW heterostructure in Fig. 9 without (a) and with (c) the consideration of SOC, respectively. The red and blue curves denote the spin-up and spin-down bands, respectively. (b), (d) Zoom in on the black dashed circles in panels (a) and (c), respectively. (e)–(h) The same as panels (a)–(d) except that the distance (vdW gap) between graphene and the $Cr_2Ge_2Te_6$ sheet is reduced by 0.3 Å ($d = 3.26$ Å). Reprinted with permission from Ref. [18]. Copyright 2015 by the American Physical Society.

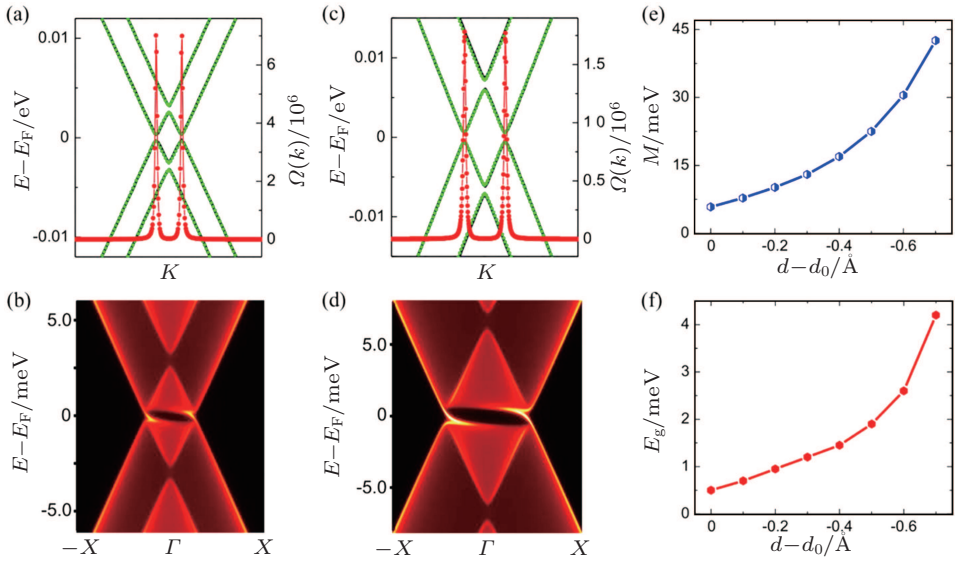


Fig. 11. (color online) (a) The calculated Berry curvature (red) for the whole valence bands. The black curves and green dots denote the band structures obtained from the DFT calculations and the TB model, respectively. (b) The calculated edge density of states for the armchair edge of the semi-infinite system. (c) and (d) The same as panels (a) and (b) except that the distance (vdW gap) between graphene and the $Cr_2Ge_2Te_6$ sheet is reduced by 0.3 Å ($d = 3.26$ Å). (e) The induced exchange splitting (M) in the graphene layer as a function of $d - d_0$, where d is the vdW distance between graphene and the $Cr_2Ge_2Te_6$ sheet and d_0 is the corresponding optimized vdW distance ($d_0 = 3.56$ Å). (f) The SOC induced band gap E_g as a function of $d - d_0$. Reprinted with permission from Ref. [18]. Copyright 2015 by the American Physical Society.

The proximity coupling effect in the vdW heterostructure can be enhanced by reducing the distance between graphene and the substrate. Due to the weak vdW interaction, the distance between graphene and the FM substrate $Cr_2Ge_2Te_6$ can be easily reduced in experiments by applying an external pressure. Figures 11(e) and 11(f) show that the exchange field and the QAH gap can be increased significantly through reducing the vdW gap. The nontrivial QAH gap is increased to 4.3 meV when the vdW gap is reduced by 0.7 Å. The size of the gap corresponds to a temperature of about 50.0 K, promising for experimental observation of the QAH effect in high temperature. The robustness of the achieved QAH effect is confirmed by investigating the electronic and topological behaviors of the heterostructure with other combination configurations, which means that the QAH effect in the vdW heterostructure is independent of the stacking patterns and can be easily realized in experiments as long as the graphene is placed on the top of the $Cr_2Ge_2Te_6$ sheet, superior to other theoretical models

proposed to realize the QAH effect in graphene. Based on the above graphene-based vdW heterostructure, a brand new multichannel or high Chern number QAH device prototype made of alternating $Cr_2Ge_2Te_6$ and graphene is proposed, supporting dissipationless edge conducting transport with a quantized conductivity of $2N \times e^2/h$, where N is the number of graphene layers in the system. Thus, the graphene-based vdW heterostructure is a perfect system to observe the QAH effect with currently experimental technologies and may greatly push the experimental study of the QAH effect.[18]

4. QAH effect in silicene-based systems

Silicene, a monolayer of silicon atoms with a two-dimensional honeycomb lattice, is closely analogous to graphene and has been synthesized in experiments.[56,57] Silicene also possesses the Dirac electronic properties and is predicted to be a 2D topological insulator (QSH insulator).[58] In contrast to graphene, silicene is in a low buckled honeycomb structure with the two sublattices in different planes, which leads to the relatively large SOC gap of 1.55 meV.[58] Similar to graphene, the QAH effect can also be realized in silicene through introducing magnetism and Rashba SOC.[19] Recent first-principles calculations demonstrated that silicene decorated with proper TM atoms at the hollow adsorption site can realize the QAH effect.[20,21] The adsorption energies of the TM atoms adsorbed on silicene are much larger than those on graphene, indicating strong structural stability of silicene decorated with TM atoms and the TM atoms generally do not form into clusters when they are deposited on the silicene sheet. The mechanism of the QAH effect in silicene with TM atoms adsorbed at the hollow site can be explained by the following TB model. In this model, the TM induced exchange field, the staggered AB-sublattice potential, and the extrinsic Rashba SOC are only considered for the Si atoms nearest to the TM adatoms. The TB Hamiltonian can be written as[19,20]

$$\begin{aligned} H = & -t \sum_{\langle i,j\rangle\alpha} c^{\dagger}_{i\alpha} c_{j\alpha} + \mathrm{i}\frac{\lambda_{\mathrm{so}}}{3\sqrt{3}} \sum_{\langle i,j\rangle\alpha\beta} v_{ij} c^{\dagger}_{i\alpha} \sigma^{z}_{\alpha\beta} c_{j\beta} \\ & - \mathrm{i}\frac{2}{3}\lambda_{\mathrm{R1}} \sum_{\langle\langle i,j\rangle\rangle\alpha\beta} \mu_i c^{\dagger}_{i\alpha} \left(\boldsymbol{\sigma} \times \hat{\boldsymbol{d}}_{ij}\right)^{z}_{\alpha\beta} c_{j\beta} \\ & + \mathrm{i}\lambda_{\mathrm{R2}} \sum_{\langle m,n\rangle\alpha\beta} c^{\dagger}_{m\alpha} \left(\boldsymbol{\sigma} \times \hat{\boldsymbol{d}}_{ij}\right)^{z}_{\alpha\beta} c_{n\beta} \\ & + \sum_{m\alpha} \mu_m U c^{\dagger}_{m\alpha} c_{m\alpha} + M \sum_{m\alpha\beta} c^{\dagger}_{m\alpha} \sigma^{z}_{\alpha\beta} c_{m\beta}, \end{aligned} \tag{3}$$

where $c^{\dagger}_{i\alpha}$ ($c_{i\alpha}$) creates (annihilates) an electron with spin α on site i, $\langle i,j\rangle$ ($\langle\langle i,j\rangle\rangle$) runs over all the nearest (next-nearest) neighbor hopping sites, $\boldsymbol{\sigma}$ is the Pauli matrix, $v_{ij} = \pm 1$ if the next-nearest-neighboring hopping is counterclockwise (clockwise) with respect to the positive c axis, and symbols m, n refer to the sites nearest to the TM atom. The first term represents the nearest-neighboring hopping with amplitude t, and the second term is the intrinsic SOC. The third term describes the intrinsic Rashba SOC arising from the low-buckled structure of silicene, where $\boldsymbol{d}_{ij}$ denotes the lattice vector pointing from site j to site i in the same sublattice and $\mu_i = \pm 1$ for the A-type (B-type) site. The last three terms represent the extrinsic Rashba SOC, the staggered AB-sublattice potential, and the magnetic exchange field, respectively, all induced by the TM atoms. The TM-induced extrinsic Rashba SOC is usually much larger than the other two SOC terms. Figure 12(a) plots the band structure of pristine silicene with the perfect spin degenerate Dirac bands at the K (K') point. When the TM-induced staggered AB-sublattice potential U is present, a trivial bulk band gap is opened at the Dirac points, as shown in Fig. 12(b). When the magnetic exchange field is taken into account, the spin degenerate states will split into the spin-up and spin-down Dirac bands. If the exchange field is strong enough, the trivial band gap induced by the staggered AB-sublattice potential will disappear, and the spin-up and spin-down Dirac bands will cross with each other, as displayed in Fig. 12(c). Then, a new band gap can be opened around the K and K' Dirac points after the Rashba SOC is included (Fig. 12(d)). Due to the inequivalence of the A and B sublattices in TM-silicene, the sizes of the gaps opened by the Rashba SOC around the K and K' points are not equal to each other. Similar to the case of graphene, these SOC-induced band gaps are topologically nontrivial and the obtained insulting state is the QAH state.[20]

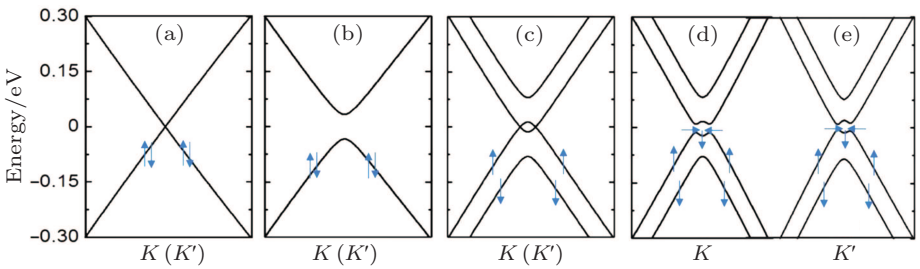


Fig. 12. (color online) Band structures calculated by using TB models with silicene hopping strength $t = 1.6$ eV. The parameters adopted are (a) $U = M = 0.0$ eV; (b) $U = 0.18$ eV, $M = 0.0$ eV; and (c) $U = 0.18$ eV, $M = 0.25$. When the SOC is included, bands in panel (d) are obtained. The arrows in panel (d) represent the spin directions. Reprinted with permission from Ref. [20]. Copyright 2013 by the American Physical Society.

The band evolution obtained from the above TB model illustrates clearly how the QAH effect can be realized in the TM atoms decorated silicene system in the present of staggered AB-sublattice potential, exchange field, and Rashba SOC. Here, we take the 4d TM Nb decorated silicene system (Nb–silicene) as an example to illustrate how the QAH effect is achieved in the real system.[20] The DFT band structure of pristine silicene without SOC is shown in Fig. 13(a), and the linear Dirac dispersion appears at the K and K' points. The slight structural distortion induced by the adsorption of Nb atoms at the hollow sites of silicene induces a band gap of about 26.5 meV at Dirac points K and K', which is obtained by calculating the band structure of the distortion silicene without Nb atoms. For the Nb–silicene system, the trivial gap at the K and K' Dirac points is enhanced to 50.3 meV (Fig. 13(b)) due to the local staggered AB-sublattice potential induced by the Nb atoms. When the spin polarization is included in the calculations, obvious spin splitting appears (Fig. 13(c)). The magnetic exchange field is much larger than the induced staggered potential, resulting in the crossing of spin-up and spin-down Dirac bands around E_F (as shown in Fig. 13(c)). When the SOC is considered, the band gaps appear at the band crossing points. The SOC-induced local gaps around the K and K' points are 18 meV and 10 meV (Fig. 13(d)), respectively. Thus, a global gap of about 10 meV is opened. Namely, a SOC-induced insulating state appears in the Nb–silicene system. This gap is opened by the Rashba-type SOC. The calculated magnetic anisotropic energies of the system show that the SOC ground state has the out-of-plane spin orientation, also important to observe the QAH effect.[20]

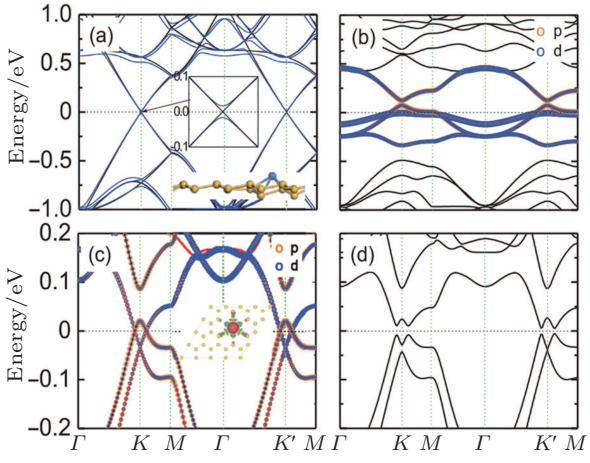


Fig. 13. (color online) (a) Band structures for pristine (black curves) and deformed (blue curves) silicene with a 4×4 supercell. In the deformed case, the Nb atoms are removed. Insets: magnified bands near the K points and the optimized structure around the Nb. (b) and (c) The band structures of silicene adsorbed with Nb without (b) and with (c) the consideration of spin polarization, respectively. The contributions from Si 3p/Nb 4d states to the bands are denoted by the orange/blue circles. The inset in panel (c) is the spatial distribution of the spin difference. (d) The corresponding bands of panel (c) with the SOC. The E_F is set at energy zero. Reprinted with permission from Ref. [20]. Copyright 2013 by the American Physical Society.

Since the adsorption energies of TM atoms on silicene are large and the TM atoms generally do not form into clusters, one may expect the realization of the QAH effect through adsorbing TM atoms on silicene is easier in experiments, compared to graphene. There are, however, other difficulties in the system. Due to the absence of the freestanding silicene in nature, the silicene is usually grown on metal substrates in experiments, which will absolutely destroy the original QAH effect. Thus, to realize the QAH effect in TM decorated silicene systems in experiments, some suitable insulating substrates must be first designed for silicene. For graphene, the freestanding monolayer exists in nature and has been fabricated successfully in experiments. According to the above discussion, the QAH effect in graphene systems can hopefully be realized in experiments by forming graphene-based heterostructures, especially the vdW-heterostructure, through depositing a graphene sheet on suitable magnetic insulating substrates.

5. QAH effect in various other material systems

Besides the typical systems of HgTe QWs, $(Bi,Sb)_2Te_3$ thin films, graphene (heterostructures), and silicene, etc., QAH effects have been reported in many other material systems, including 2D organic topological insulators,[22] heavy atomic layers on magnetic insulators,[23] (111) bilayers of $LaCoO_3$,[25] GdO/EuO quantum wells,[26] interfaces between thin films of the topologically trivial FM insulators EuO and GdN,[27] (001) double-perovskite monolayers via intersite spin–orbit coupling,[28] and so on.

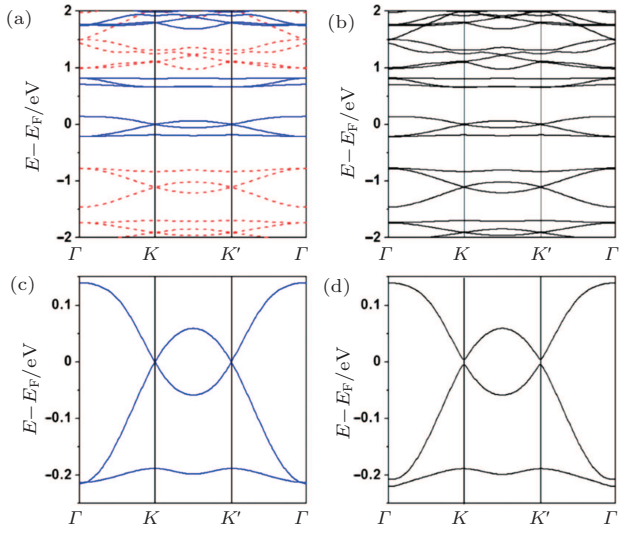


Fig. 14. (color online) (a) and (b) Band structures of the TMn lattice without and with SOC, respectively. The red (blue) dashed curves denote spin-up (spin-down) bands. (c) and (d) Magnification of panels (a) and (b) around E_F, respectively. Reprinted with permission from Ref. [22]. Copyright 2013 by the American Physical Society.

Wang *et al.* proposed that the QAH effect can be realized in a family of 2D organic topological insulators which are de-

signed by assembling molecular building blocks of triphenyl-transition-metal compounds into a hexagonal lattice and using the triphenyl-manganese (TMn) as a model system with the Mn atoms forming a honeycomb lattice.[22] Figure 14 shows the band structures of the TMn lattice. The ground state of the TMn lattice is FM with a magnetic moment of 4 μ_B per unit cell, in which the spin-up and spin-down Dirac bands are completely split away from each other with E_F located exactly at the Dirac points of the spin-down Dirac band (Figs. 14(a) and 14(c)). When the SOC is included, a topologically non-trivial bulk band gap (9.5 meV) is opened at the K and K' Dirac points around E_F (Figs. 14(b) and 14(d)), and the physical origin of the QAH effect in this system is due to the strong magnetization and intrinsic SOC provided by the honeycomb Mn atoms.[22]

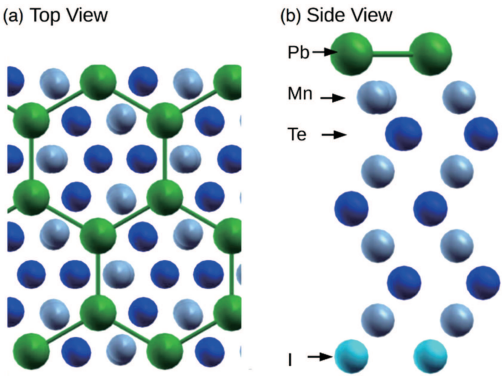


Fig. 15. (color online) (a) Top view and (b) side view of the tripled surface unit cell of MnTe with 2/3 ML Pb. Pb is in green, Mn is in gray, Te is in dark blue, and I is in cyan. Reprinted with permission from Ref. [23]. Copyright 2013 by the American Physical Society.

A large gap QAH effect was predicted to be realized by depositing atomic layers of heavy atoms (Pt–Bi) with large SOC on the surface of magnetic insulators (such as MnTe, MnSe, and EuS) (Fig. 15). The difficulties related to magnetic dopants and disorder can be avoided by the large-band-gap magnetic substrate with naturally aligned spins.[23] Based on *ab initio* calculations, Wu *et al.* proposed a large energy gap QAH effect in the half-passivated stanene (340 meV) and germanene (60 meV) systems.[24] The ferromagnetism in these 2D honeycomb materials is introduced by controlling the surface functionality instead of TM doping, wherein one sublattice is fully passivated by halide atoms while the other is not (Fig. 16) and the FM order is realized on the unpassivated sublattice. Wang *et al.* found that the interplay between SOC and Coulomb interaction stabilizes a very robust FM insulator phase with a nonzero Cherm number in the bilayer system of $LaCoO_3$ grown along the (111) direction on $SrTiO_3$, indicating the possibility of experimental observation of the QAH effect in perovskite systems.[25]

The QSH effect in the InAs/GaSb quantum well (QW) is due to the relative band inversion between the two different materials. Zhang *et al.* showed that the above relative band inversion mechanism could also be applied to oxide heterojunctions, and proposed that the QAH state could be realized in the $(CdO)_n(EuO)_m$ QW (Fig. 17).[26] The n and m represent the numbers of atomic layers of (CdO) and (EuO), respectively, and the band gap of the QW can be tuned by varying the layer thickness (n,m). EuO is an important high T_C (around 69 K) FM insulator. And a high T_C is expected for the $(CdO)_n(EuO)_m$ QW. Thus, the $(CdO)_n(EuO)_m$ QW was proposed to realize the QAH effect without random magnetic doping, which is distinct from the magnetically doped topological insulators.[26] The first-principles calculations demonstrated that an interface between thin films of the topologically trivial FM insulators EuO and GdN could also result in the QAH effect,[27] as shown in Fig. 18. The above proposal shows that the QAH effect can also be realized in the square lattice, going beyond the ordinary honeycomb lattice material systems.

Liang *et al.* demonstrated that the topological states could also be realized in a triangular lattice.[59] They found that, because of the C_3 and time reversal symmetries, p_x and p_y orbitals accommodated on the triangular lattice exhibit a quadratic band touching at the Γ point at E_F. When the SOC is included, a gap will be opened at the touching point, which results in a QSH effect state. Thus, if the time reversal symmetry of the triangular lattice system is broken by a large magnetic exchange field, the QAH effect with $C = \pm 1$ will be achieved.

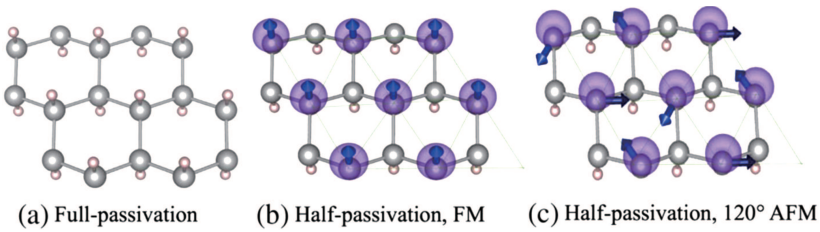


Fig. 16. (color online) Structures of stanene with (a) full- and (b)–(c) half-passivation by I atoms. Large gray and small pink spheres represent the Sn and I atoms, respectively. For the half-passivated stanene, unpassivated Sn sites exhibit magnetic moments in a triangular lattice (dotted lines), which are indicated by the blue arrows. The FM and 120° AFM phases are indicated in panels (b) and (c), respectively. The spin charge density is shown in an isovalue surface plot, which distributes primarily at the unpassivated Sn atoms. The isovalue of the spin density is chosen as 0.006 electron/Å^3. Reprinted with permission from Ref. [24]. Copyright 2014 by the American Physical Society.

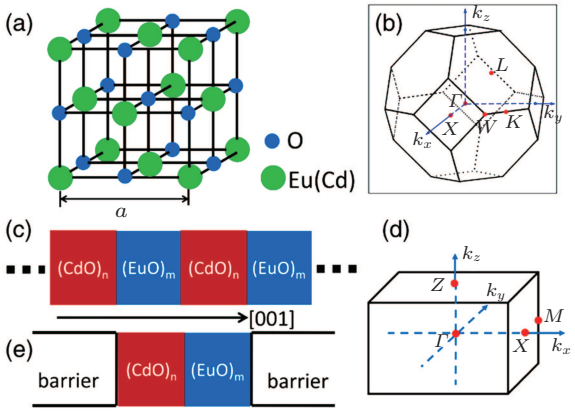


Fig. 17. (color online) (a) The rocksalt crystal structure of CdO and EuO with space group $Fm\bar{3}m$ (No. 255). (b) The Brillouin zone for the rocksalt structure. The time-reversal invariant momentum points are marked, for example, $\Gamma(0,0,0)$, $X(\pi,\pi,0)$, and $L(\pi,0,0)$. (c) The schematic of the $(CdO)_n(EuO)_m$ superlattice. (d) The BZ of the $(CdO)_n(EuO)_m$ superlattice. (e) The schematic of the $(CdO)_n(EuO)_m$ quantum Well. Reprinted with permission from Ref. [26]. Copyright 2014 by the American Physical Society.

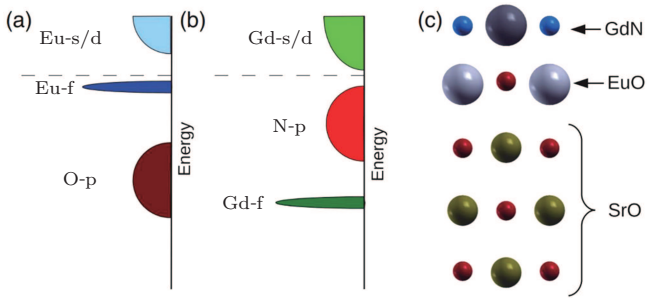


Fig. 18. (color online) Schematic densities of states of (a) EuO and (b) GdN. (c) Side view of the proposed interface structure composed of one GdN layer atop one EuO layer on a SrO substrate. Large atoms are cations (Gd, Eu, and Sr), and small atoms are anions (N and O). Reprinted with permission from Ref. [27]. Copyright 2014 by the American Physical Society.

6. New quantum states related to the QAH state

The valley-polarized quantum anomalous Hall state and the quantum spin-quantum anomalous Hall state are the QAH-related new topological states, where two different quantum states coexist in a material system. The valley degree of freedom in the honeycomb lattice system is essential for the application of valleytronics.[60] Silicene has a honeycomb geometry and a low-buckled structure. By breaking the inversion symmetry of silicene, e.g., by introducing a relatively large staggered AB-sublattice potential, a bulk band gap can be opened at the K and K' points and the quantum valley Hall (QVH) effect can be obtained, characterized by the valley Chern number $C_v = C_k - C'_k$.[61] As shown in Eq. (3), the coexistence of intrinsic and extrinsic Rashba SOCs in silicene may generate a new type of topological phase due to their different responses at the valleys K and K'. Through tuning these Rashba SOCs in silicene, Pan *et al.* numerically found a new quantum state, the valley-polarized quantum anomalous Hall (VP-QAH) state, in which the quantum valley Hall state (valley Chern number $C_v = 3$, where $C_k = 1$ and $C'_k = -2$) and the quantum anomalous Hall state (Chern number $C = -1$) coexist in the material,[61] as shown in Fig. 19. Based on the first-principles calculations, Liu *et al.* reported the theoretical finding of the novel VP-QAH phase with a large band gap of 0.19 eV in half-hydrogenated Bi honeycomb monolayers.[62]

Ezawa reported from TB models that the topological properties of silicene could also be tuned by applying the staggered exchange field $\Delta M = M_A - M_B$, where M_A and M_B are the magnetic exchange fields operating on the A and B sublattices, respectively.[63] The QSH state and the QAH state are the well-known topologically protected states, which are characterized by the helical and the chiral gapless edge states, respectively. By introducing the staggered magnetic exchange field ΔM, the author discovered a new hybrid topological state, the quantum spin-quantum anomalous Hall (QSQAH) state, where the two different topological states coexist, i.e., the QSH effect is realized at one valley (K point) while the QAH effect is realized at the other valley (K' point).[63] The topological numbers of QSQAH are given by one half of the sum of those of the QAH and QSH states: Chern number $C = \pm 1$ and spin Chern number $C_s = 1/2$. Based on the first-principles calculations, Zhou *et al.* reported the novel QSQAH effect in the Sb(111) monolayers decorated with H and certain magnetic atoms.[64] The drastic exchange field induced by the decoration of H atoms and magnetic (Cr/Mo/W) atoms at the A and

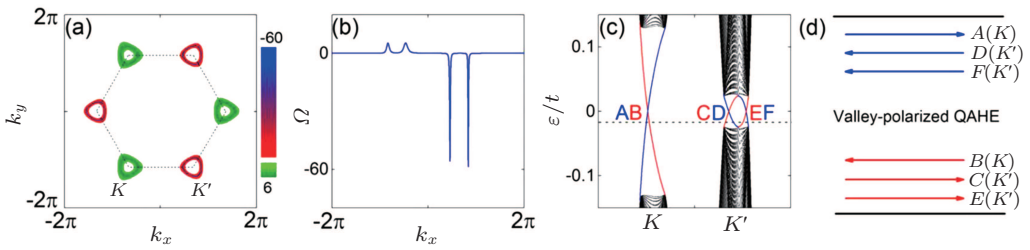


Fig. 19. (color online) (a) Contour of Berry curvature distribution in (k_x, k_y) plane for the valley-polarized QAH effect. (b) Berry curvature distribution as a function of k_x at fixed $k_y = 2\pi/\sqrt{3}$. (c) The band structure of zigzag-terminated silicene exhibiting the valley-polarized QAH effect, where colors are used to label the edge modes localized at the opposite boundaries. (d) Valley-associated edge modes for the valley-polarized QAH effect. Reprinted with permission from Ref. [61]. Copyright 2014 by the American Physical Society.

Table 1. Summary of the material systems proposed for realizing the QAH effect. The listed contents include the material systems, the Chern numbers obtained in the systems, the important characteristics, the QAH gaps, and the corresponding references.

Material system	Chern number C	Description	QAH gap/meV	Ref.
HgTe QWs	1	magnetic doping		[9]
p–n junction QWs	1	magnetic doping	~ 5	[10]
Magnetic TIs thin film	1	magnetic doping		[11]
TM atoms/graphene	2, –2	TM atom adsorption	$\sim$ 1–100	[12]–[15]
graphene/$BiFeO_3$(111)	2	AFM insulator substrate	$\sim$ 1–4	[16]
graphene/$RbMnCl_3$(001)	2	AFM insulator substrate	$\sim$ 1–9	[17]
graphene/$Gr_2Ge_2Te_6$	2	FM insulator substrate, vdW heterostructure	$\sim$ 1–4	[18]
TM atoms/silicene	2, –2, 1	TM atom adsorption	$\sim$ 1–10	[19]–[21]
2D organic TIs	1	Mn honeycomb lattice, intrinsic	~ 9.5	[22]
(111) bilayer of oxides ($LaCoO_3$, $LaNiO_3$, $SrIrO_3$)	1, 2	heterostructure		[25], [32], [33]
CdO/EuO	1	quantum wells	~ 20	[26]
GdN/EuO	1	interface	~ 100	[27]
Pb/MnTe	–1	magnetic substrate	~ 36	[23]
I-germanene, I-stanene	1	half-passivated	$\sim$ 60–340	[24]
H-Bi(111)	1	half-hydrogenated	~ 200	[62]
Functionalized Sb(111)	1	H and TM atoms decorated	$\sim$ 20–50	[64]
LaX (X = Br, Cl, I)	1	intrinsic	$\sim$ 14–25	[29]
$HgCr_2Se_4$		thin film, intrinsic		[30]
Double perovskites	2, –2	heterostructure	$\sim$ 0.1–26	[28], [31]
Topological crystalline insulator	between –4 and 4	thin-film and FM doping		[34]

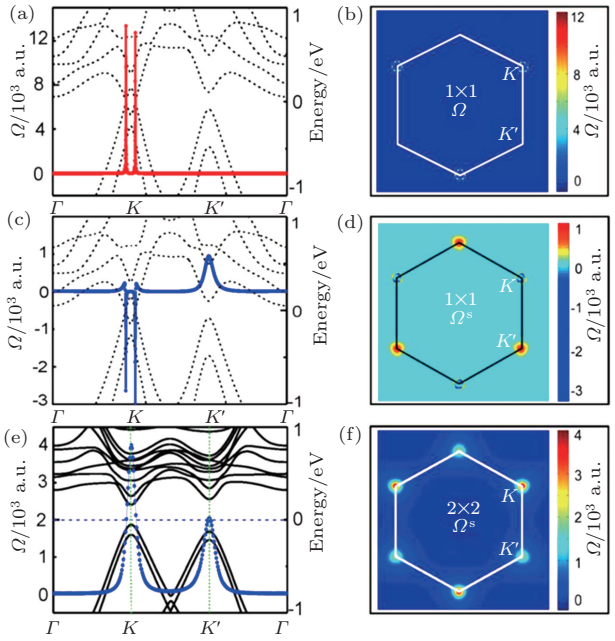


Fig. 20. (color online) (a) Berry curvatures (red dots) for the whole valence bands (in atomic units (a.u.)) of Mo@SbH in the case of 1×1 unit cell, with a 3% tensile strain applied. The corresponding band structures (black dashed curves) are also displayed. (b) The distributions of the Berry curvatures in 2D momentum space for the same system in panel (a). (c) and (d) The same as those in panels (a) and (b), respectively, except for spin Berry curvatures (blue dots in (c)) instead. (e) and (f) The same as those in panels (c) and (d), except for the case of 2×2 supercell. The bands in panel (e) are shown by black solid curves. In panels (e) and (f), no strain is applied. Reprinted with permission from Ref. [64]. Copyright 2015 by the American Chemical Society.

B sublattices of the honeycomb Sb(111) monolayers, together with the strong SOC of the Sb atoms, generates the novel QSQAH state.[64] Figure 20 shows the band structures and (spin) Berry curvatures obtained from the *ab initio* calculations, associated with the obtained Chern number of 1 and spin Chern number of $\sim 1/2$, which clearly illustrate the realization of the QSQAH effect in the functionalized Sb(111) monolayers.[64]

The material systems proposed for realizing the QAH effect have been summarized in Table 1, where the Chern numbers and the QAH gaps obtained in the systems are also given. The important characteristics of the systems are also briefly introduced. The last column displays the corresponding references. From the table, one can see that the half-passivated Sn or Bi systems can give the QAH effect with very large gaps. They may be ideal systems to observed the QAH effect, if the sample fabrication can be easily realized in experiments.

7. Conclusions and outlook

In this review, we systematically discussed the theoretical proposals for realizing the QAH effect in various real material systems. The theoretical studies demonstrate that the QAH effect can be realized in the TRS broken QSH insulator HgTe QWs and tetradymite semiconductors Bi_2Te_3, Bi_2Se_3, and Sb_2Te_3 by doping magnetic atoms. By introducing Rashba SOC and a magnetic exchange field, graphene and silicene are suitable prototype materials for engineering the QAH effect. The QAH effect can also be realized in various other real materials, such as 2D organic topological insulators, heavy atomic layers on magnetic insulators, GdO/EuO quantum wells, (111) bilayers of $LaCoO_3$, and so on. Two QAH-based novel topological states, VP-QAH state and QSQAH state, were also discussed in this work. Although there are plenty of theoretical proposals, the QAH effect has solely been observed in experiments in thin films of magnetically doped topological insulators ($(Bi, Sb)_2Te_3$) at an extremely low temperature. It is generally not very easy to synthesize the proposed material systems theoretically, which makes the experimental realization of the QAH effect challenging. Thus, to realize the

QAH effect straightforward in experiments, the proposed system must be robust against disorder and easy to be synthesized, where a high T_C and a relatively large bulk band gap are also required. When compared to the other materials in the theoretical proposals, graphene is the most stable 2D material and relatively mature to be fabricated in experiments, which indicates that the robust QAH effect proposed in the graphene-based vdW heterostructure may be the most perfect candidate system for experimental observation of the QAH effect up to the present. Further, to apply the QAH effect in future low-power-consumption electronic devices, the room-temperature QAH state must be achieved in certain material systems, which calls for more effort on the experimental and theoretical studies in this significant direction.

References

[1] Hasan M Z and Kane C L 2010 *Rev. Mod. Phys.* **82** 3045
[2] Qi X L and Zhang S C 2011 *Rev. Mod. Phys.* **83** 1057
[3] He K, Wang Y Y and Xue Q K 2014 *Natl. Sci. Rev.* **1** 138
[4] He K, Ma X C, Chen X, Lu L, Wang Y Y and Xue Q K 2013 *Chin. Phys. B* **22** 067305
[5] Gao C L, Qian D, Liu C H, Jia J F and Liu F 2013 *Chin. Phys. B* **22** 067304
[6] Liu Z, Liu F and Wu Y S 2014 *Chin. Phys. B* **23** 077308
[7] Klitzing K V, Dorda G and Pepper M 1980 *Phys. Rev. Lett.* **45** 494
[8] Haldane F D M 1988 *Phys. Rev. Lett.* **61** 2015
[9] Liu C X, Qi X L, Dai Xi, Fang Z and Zhang S C 2008 *Phys. Rev. Lett.* **101** 146802
[10] Zhang H J, Xu Y, Wang J, Chang K and Zhang S C 2014 *Phys. Rev. Lett.* **112** 216803
[11] Yu R, Zhang W, Zhang H J, Zhang S C, Dai X and Fang Z 2010 *Science* **329** 61
[12] Qiao Z H, Yang S A, Feng W X, Tse W K, Ding J, Yao Y G, Wang J and Niu Q 2010 *Phys. Rev. B* **82** 161414(R)
[13] Qiao Z H, Jiang H, Li Z, Yao Y G and Niu Q 2012 *Phys. Rev. B* **85** 115439
[14] Ding J, Qiao Z H, Feng W X, Yao Y G and Niu Q 2011 *Phys. Rev. B* **84** 195444
[15] Zhang H B, Lazo C, Blügel S, Heinze S and Mokrousov Y 2012 *Phys. Rev. Lett.* **108** 056802
[16] Qiao Z H, Ren W, Chen H, Bellaiche L, Zhang Z Y, MacDonald A H and Niu Q 2014 *Phys. Rev. Lett.* **112** 116404
[17] Zhang J Y, Zhao B, Yao Y G and Yang Z Q 2015 *Sci. Rep.* **5** 10629
[18] Zhang J Y, Zhao B, Yao Y G and Yang Z Q 2015 *Phys. Rev. B* **92** 165418
[19] Ezawa M 2012 *Phys. Rev. Lett.* **109** 055502
[20] Zhang J Y, Zhao B and Yang Z Q 2013 *Phys. Rev. B* **88** 165422
[21] Zhang X L, Liu L F and Liu W M 2013 *Sci. Rep.* **3** 2908
[22] Wang Z F, Liu Z and Liu F 2013 *Phys. Rev. Lett.* **110** 196801
[23] Garrity K F and Vanderbilt D 2013 *Phys. Rev. Lett.* **110** 116802
[24] Wu S C, Shan G C and Yan B H 2014 *Phys. Rev. Lett.* **113** 256401
[25] Wang Y L, Wang Z J, Fang Z and Dai X 2015 *Phys. Rev. B* **91** 125139
[26] Zhang H J, Wang J, Xu G, Xu Y and Zhang S C 2014 *Phys. Rev. Lett.* **112** 096804
[27] Garrity K F and Vanderbilt D 2014 *Phys. Rev. B* **90** 121103(R)
[28] Zhang H B, Huang H Q, Haule K and Vanderbilt D 2014 *Phys. Rev. B* **90** 165143
[29] Dolui K, Ray S and Das T 2015 *Phys. Rev. B* **92** 205133
[30] Xu G, Weng H M, Wang Z J, Dai X and Fang Z 2011 *Phys. Rev. Lett.* **107** 186806
[31] Cook A M and Paramekanti A 2014 *Phys. Rev. Lett.* **113** 077203
[32] Wang F and Ran Y 2011 *Phys. Rev. B* **84** 241103(R)
[33] Yang K Y, Zhu W G, Xiao Di, Okamoto S, Wang Z and Ran Y 2011 *Phys. Rev. B* **84** 201104(R)
[34] Fang C, Gilbert M J and Bernevig B A 2014 *Phy. Rev. Lett.* **112** 046801
[35] Chang C Z, Zhang J S, Feng X, Shen J, Zhang Z C, Guo M H, Li K, Ou Y B, Wei P, Wang L L, Ji Z Q, Feng Y, Ji S H, Chen X, Jia J F, Dai X, Fang Z, Zhang S C, He K, Wang Y Y, Lu L, Ma X C and Xue Q K 2013 *Science* **340** 167
[36] Checkelsky J G, Yoshimi R, Tsukazaki A, Takahashi K S, Kozuka Y, Falson J, Kawasaki M and Tokura Y 2014 *Nat. Phys.* **10** 731
[37] Kou X F, Guo S T, Fan Y B, Pan L, Lang M R, Jiang Y, Shao Q M, Nie T X, Murata K C, Tang J S, Wang Y, He L, Lee T K, LeeWL andWang K L 2014 *Phys. Rev. Lett.* **113** 137201
[38] Chang C Z, Zhao W W, Kim D Y, Zhang H J, Assaf B A, Heiman D, Zhang S C, Liu C X, Chan M H W and Moodera J S 2015 *Nat. Mater.* **14** 473
[39] Bernevig B A, Hughes T L and Zhang S C 2006 *Science* **314** 1757
[40] König M, Wiedmann S, Brüne C, Roth A, Buhmann H, Molenkamp L W, Qi X L and Zhang S C 2007 *Science* **318** 766
[41] Zhang H J, Liu C X, Qi X L, Dai X, Fang Z and Zhang S C 2009 *Nat. Phys.* **5** 438
[42] Thouless D J, Kohmoto M, Nightingale M P and den Nijs M 1982 *Phys. Rev. Lett.* **49** 405
[43] Chang M C and Niu Q 1996 *Phys. Rev. B* **53** 7010
[44] Yao Y G, Kleinman L, MacDonald A H, Sinova J, Jungwirth T, Wang D S, Wang E and Niu Q 2004 *Phys. Rev. Lett.* **92** 037204
[45] Yao Y G, Ye F, Qi X L, Zhang S C and Fang Z 2007 *Phys. Rev. B* **75** 041401(R)
[46] Gmitra M, Konschuh S, Ertler C, Ambrosch-Draxl C and Fabian J 2009 *Phys. Rev. B* **80** 235431
[47] Ma D W, Li Z Y and Yang Z Q 2012 *Carbon* **50** 297
[48] Eelbo T, Waśmiowska M, Thakur P, Gyamfi M, Sachs B, Wehling T O, Forti S, Starke U, Tieg C, Lichtenstein A I and Wiesendanger R 2013 *Phys. Rev. Lett.* **110** 136804
[49] Chen H, Niu Q, Zhang Z Y and MacDonald A H 2013 *Phys. Rev. B* **87** 144410
[50] Luo W D and Qi X L 2013 *Phys. Rev. B* **87** 085431
[51] Geim A K and Grigorieva I V 2013 *Nature* **499** 419
[52] Avsar A, Tan J Y, Taychatanapat T, Balakrishnan J, Koon G K W, Yeo Y, Lahiri J, Carvalho A, Rodin A S, O'Farrell E C T, Eda G, Castro Neto A H and Özyilmaz B 2014 *Nat. Commun.* **5** 4875
[53] Carteaux V, Brunet D, Ouvrard G and André G 1995 *J. Phys.: Condens. Matter* **7** 69
[54] Alegria L D, Ji H, Yao N, Clarke J J, Cava R J and Petta J R 2014 *Appl. Phys. Lett.* **105** 053512
[55] Ji H, Stokes R A, Alegria L D, Blomberg E C, Tanatar M A, Reijnders A, Schoop L M, Liang T, Prozorov R, Burch K S, Ong N P, Petta J R and Cava R J 2013 *J. Appl. Phys.* **114** 114907
[56] Lalmi B, Oughaddou H, Enriquez H, Kara A, Vizzini S, Ealet B and Aufray B 2010 *Appl. Phys. Lett.* **97** 223109
[57] Vogt P, Padova P D, Quaresima C, Avila J, Frantzeskakis E, Asensio M C, Resta A, Ealet B and Lay G L 2012 *Phys. Rev. Lett.* **108** 155501
[58] Liu C C, Feng W X and Yao Y G 2011 *Phys. Rev. Lett.* **107** 076802
[59] Liang Q F, Yu R, Zhou J and Hu X 2016 *Phys. Rev. B* **93** 035135
[60] Xiao Di, Yao W and Niu Q 2007 *Phys. Rev. Lett.* **99** 236809
[61] Pan H, Li Z S, Liu C C, Zhu G B, Qiao Z H and Yao Y G 2014 *Phys. Rev. Lett.* **112** 106802
[62] Liu C C, Zhou J J and Yao Y G 2015 *Phys. Rev. B* **91** 165430
[63] Ezawa M 2013 *Phys. Rev. B* **87** 155415
[64] Zhou T, Zhang J Y, Zhao B, Zhang H S and Yang Z Q 2015 *Nano Lett.* **15** 5149